Comparison of Whole Body Response in Oblique and Full Frontal Sled Tests

Salvador Montesinos Acosta, Joseph H. Ash, David J. Lessley, C. Greg Shaw, Sara B. Heltzel, Jeff R. Crandall

Abstract Efforts to improve restraint design for occupant protection require a detailed knowledge of human kinematic response and thoracic deformation. This study presents the spinal displacement response, thoracic deformation and restraint forces of five male post-mortem human subjects (PMHS) subjected to a simulated 30 km/h frontal collision, and three male PMHS subjected to a simulated 30 km/h near-side oblique collision. The eight PMHS approximated the 50th percentile male in both stature and mass and were restrained by a three-point belt that incorporated a custom, force-limited shoulder-belt. During the tests, a motion capture system was used to obtain the 3D displacements of the head, T1, T8, L2, pelvis and shoulders relative to the vehicle buck. Additional locations on the anterior rib cage, including the sternum, upper left, upper right, lower left and lower right rib cage, were also measured using the motion capture system and were reported relative to a spinal coordinate system based on the T8 vertebrae in order to quantify chest deflection. These data were then used to develop three-dimensional displacement corridors to quantify the whole-body kinematic response of restrained PMHS. The provided response corridors will be immediately useful for efforts to evaluate or enhance the kinematic performance of Anthropomorphic Test Devices (ATDs) and computational models. Differences in the test conditions were seen in the lateral 3D displacements with the oblique tests having higher displacements due to the lateral component of the buck acceleration.

Keywords Corridors, Frontal, Kinematics, Oblique, PMHS.

I. INTRODUCTION

Historically, occupant safety research has focused on full frontal impacts in order to define occupant response, to assess injury risk and to develop countermeasures for occupant protection. Recently, however, research efforts have begun to focus on oblique frontal collisions in order to better understand the influence that oblique impacts may have on occupant response and corresponding injury risk in comparison to full frontal impacts. While the importance of, and interest in, oblique collisions continues to rise, there is a notable absence in the literature of studies that: (1) quantify the whole-body response of a restrained occupant in an oblique impact condition; or (2) provide a detailed comparison of oblique and full frontal occupant responses. The goal of the current study is to comprehensively quantify the whole body response of restrained PMHS in both near-side oblique and full frontal impact conditions and to provide a detailed comparison of these responses.

II. METHODS

Building on the previously published Gold Standard 1 (GS1) PMHS frontal impact tests [1], two additional impact conditions were developed and utilised for the current study in order to quantify the responses of eight male PMHS. The first test condition was a full frontal 30 km/h impact using a custom 3 kN force-limited shoulder-belt and is referred to as the Gold Standard 2 (GS2) condition. The second condition was a 30 km/h, 30-degree near-side oblique frontal impact using the same custom 3 kN force-limited shoulder-belt and is referred to as the Gold Standard 3 (GS3) condition. The test conditions approximated those of a belted occupant in an actual full frontal or near-side oblique crash. In all tests, a reverse acceleration sled was used to produce the 9 g acceleration pulse used for each test (Fig. 1). All PMHS were male and approximated 50th percentile stature and mass. Five PMHS were tested in the full frontal condition, and three PMHS were tested in the oblique condition (Table I). All PMHS were tested using a passenger-side restraint configuration. Additional PMHS positioning information for the test conditions can be found in Appendices A and B.

S. Montesinos Acosta (e-mail: sm7kc@virginia.edu; tel: 1-434-297-8047) is a Research Assistant, J. Ash is a Graduate Research Assistant, D. Lessley and G. Shaw are Senior Scientists, S. Heltzel is the Anatomical Donations Coordinator and J. Crandall is the Director, all at the University of Virginia Center for Applied Biomechanics, USA.

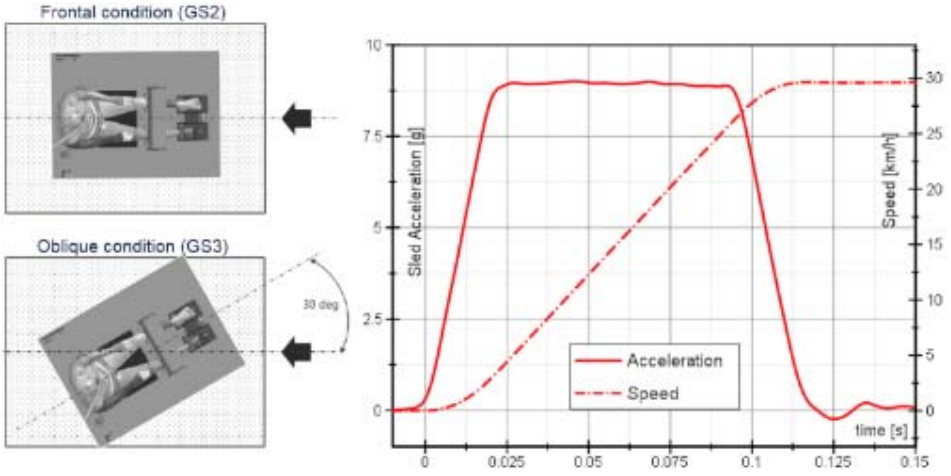

Fig. 1. Frontal condition (GS2) and oblique condition (GS3), same pulse both conditions (9 g and 30 km/h).

PMHS Considerations

The eight PMHS (Table I) were selected based on the absence of pre-existing fractures, lesions or other bone pathology, as confirmed by a computed tomography (CT) scan performed prior to the testing. The PMHS were obtained and treated in accordance with the ethical guidelines established by the National Highway Traffic Safety Administration (NHTSA, USA), and all testing and handling procedures were reviewed and approved by the University of Virginia Center for Applied Biomechanics Protocol Committee and the University of Virginia Institutional Review Board – Human Subject Use.

TABLE I
PMHS CHARACTERISTICS

	Frontal (GS2)					Oblique (GS3)		
TSTREF in NHTSA BioDB	UVAS028	UVAS029	UVAS0302	UVAS0303	UVAS0304	UVAS0313	UVAS0314	UVAS0315
Cadaver ID No.	494	492	674	736	695	632	750	767
Age at Time of Death	59	66	67	67	74	69	66	67
Sex	Male	Male	Male	Male	Male	Male	Male	Male
Body Mass (kg)	68	70	68	68	70	69	76	64
Stature (mm)	1780	1790	1770	1730	1830	1730	1715	1765
Seated Height (mm)	1120	1130	980	940	1050	1002	978	984

Motion Capture Methodology

Specific anatomical locations were selected and identified for kinematic measurement, including the head, 1st thoracic vertebra (T1), 8th thoracic vertebra (T8), 2nd lumbar vertebra (L2), pelvis and left and right shoulders. Additional points on the anterior thorax were also identified and included: sternum (ST); chest upper left (UL) and upper right (UR), located on the 4th rib approximately 45 mm from the sternal centreline along the path of the rib; and chest lower left (LL) and lower right (LR) located on the 7th rib, approximately 125 mm from the sternal centreline along the path of the rib. The identified points are illustrated in Fig. 2. At each of these measurement locations, visible four-target clusters (Fig. 3), used for measurement of translation and rotation, were surgically attached to the skull, selected vertebrae, ribs, and pelvis. The shoulders were measured with a single reflective marker placed on the skin surface superior to the acromion.

During the impact event a 16-camera, optoelectronic stereo photogrammetric system (Vicon, MX series, Oxford, UK) was used to track the trajectories of the attached target clusters. A recording frequency of 1000 Hz or 500 Hz was selected to optimize target tracking. For subsequent calculations, the data for all of the tests were analysed at 500 Hz. The recorded trajectories of the attached target clusters were used to calculate the trajectories of the underlying skull, selected vertebrae, shoulders and pelvis using a coordinate transformation and the assumption of rigid body motion as described in previous literature [2]. In addition, the tests were recorded using digital video imagers at 1000 frames per second (NAC Image Technology, Simi Valley, California).

Using the four-marker cluster trajectories provided by the motion capture system during each test, the video data analysis methods [2-3] were used to calculate transformation matrices describing the positions and

orientations of each skeletal structure with respect to a global, laboratory-fixed reference frame throughout the impact event. However, it is often more advantageous for the positions and orientations to be described relative to a moving coordinate system, such as one attached to the vehicle buck ("buck"). Thus, through matrix multiplication [3] the positions and orientations of all selected skeletal structures were described relative to the buck at each millisecond throughout the test event. The position data, calculated over the duration of the test event, provided the 3D displacements of the head, selected vertebrae, shoulders and pelvis with respect to the buck coordinate system (Fig. 4), which conformed to the recommendations set out by SAE-J211 [4]. For each measurement location, a local, anatomically based coordinate system [5] was created on the selected skeletal structure of interest. The calculated displacements are the displacements of the origins of each of these skeletal coordinate systems and are illustrated in Fig. 4. Since the subjects approximated the 50th percentile adult male anthropometry, no scaling of the displacement data was performed.

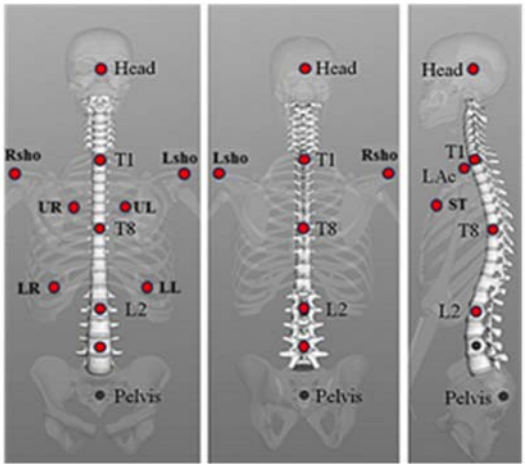

Fig. 2. Kinematic measurement locations (adapted from Ash *et al*. [1]).

Fig. 3. Subject motion capture measurement hardware.

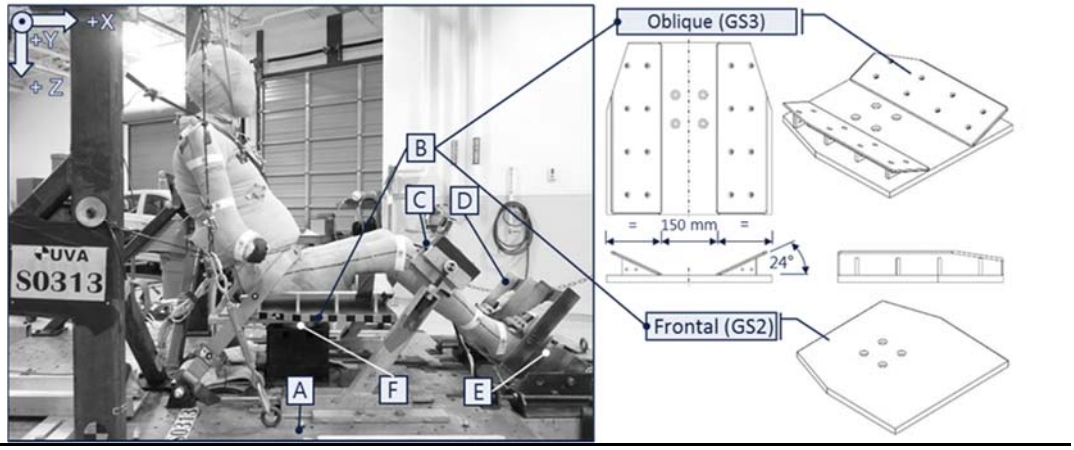

A	Buck	Restraint geometry similar to 1998 Ford Taurus front passenger position. (Oblique position 30 degrees.)
B	Seat	Rigid aluminium plate (with bilateral wedges for the oblique (GS3) tests).
C	Knee bolster	Adjustable bilateral non-padded knee channels atop six-axis load cells.
D	Footrest	Adjustable bilateral channels with ankle straps to immobilise feet and lower legs.
E	Footrest load cell	Six-axis load cell supporting footrest.
F	Seat load cell	Six-axis load cell supporting seat.

Fig. 4. Test fixture and hardware.

Subject Positioning and Test Fixture

Each subject, with implanted measurement hardware installed, was seated on a rigid horizontal seat surface and positioned into a seated posture approximating that described by Schneider *et al*. [6]. The subject was restrained by a three-point lap- and shoulder-belt in a right-front passenger configuration and was then subjected to a simulated 30 km/h frontal or oblique collision.

The test fixture (Fig. 4) and test methodology were designed to create conditions approximating those of a belted occupant in an actual full frontal or near-side oblique crash with a restrained occupant [1]. The test fixture was also designed to provide repeatable and reproducible test conditions that would allow whole-body kinematic response to be comprehensively measured and analysed. The restraint consisted of a three-point lap- and shoulder-belt with anchor positions approximating those found in a typical mid-size US sedan. The belt did not include a retractor, instead using a custom 3 kN force-limited shoulder-belt and webbing material manufactured by Narricut (International twill pattern 13195, 6–8% elongation and 6000 lbf minimum tensile strength), which was replaced for each test. Pelvis and lower extremity movements were restricted using a rigid knee bolster and footrest, which were adjusted to be in contact with the knees and feet of each subject at the beginning of the test. In the oblique condition, the seat was modified with bilateral wedges in order to reduce the risk of the pelvis sliding laterally off the seat (Fig. 4). The combination of lap-belt, knee bolster and footrest was designed to minimise pelvic and lower extremity movements during the test while allowing the characteristic forward torso motion associated with an actual automotive restraint system. In addition to whole-body kinematics, all occupant/buck interfaces were also measured. The measured occupant interfaces included X-axis, Y-axis and Z-axis forces and moments on the seat, footrest and each knee bolster, as well as standard lap- and shoulder-belt load measurements (Fig. 4).

Corridor construction

For each skeletal measurement location the X-axis, Y-axis and Z-axis displacements were obtained with respect to the buck for each subject at two millisecond intervals. The chest displacement corridors are with respect to the T8 coordinate system. An average, and one standard deviation (±1 S.D.) corridor above and below the average, was created for each displacement location (e.g. X-axis head displacement) for each test condition for each point in time. This process creates a corridor (±1 S.D.) around the average value of each displacement at each point in time and is shown in Fig. 5.

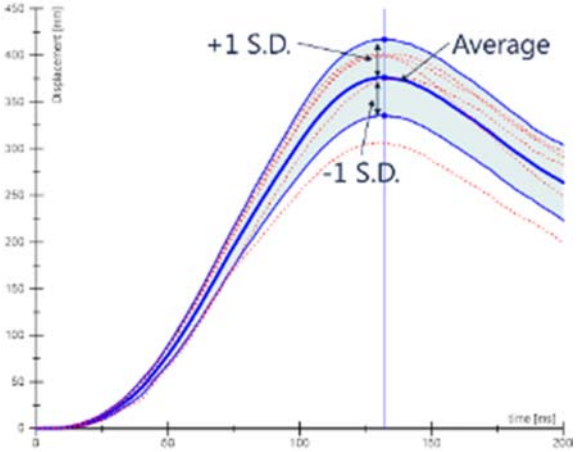

Fig. 5. Corridor construction.

This process was repeated for the X-axis, Y-axis and Z-axis displacement components for each of the eight measurement locations to determine a total of 21 skeletal displacement corridors, 15 thorax displacement corridors and 15 restraint forces displacement corridors for the five subjects in GS2 and the three subjects in GS3 in order to create two sets of corridors.

III. RESULTS

Five 30 km/h frontal tests and three oblique tests (Figs 6 and 7) were performed using eight restrained PMHS. During each test, skeletal kinematic data were successfully collected for the head, T1, T8, L2, shoulders, ribs and pelvis at every other millisecond during the impact event. Occupant interface loads and moments were

also collected successfully (Fig. 4). From these data, displacement response and occupant interface corridors were constructed.

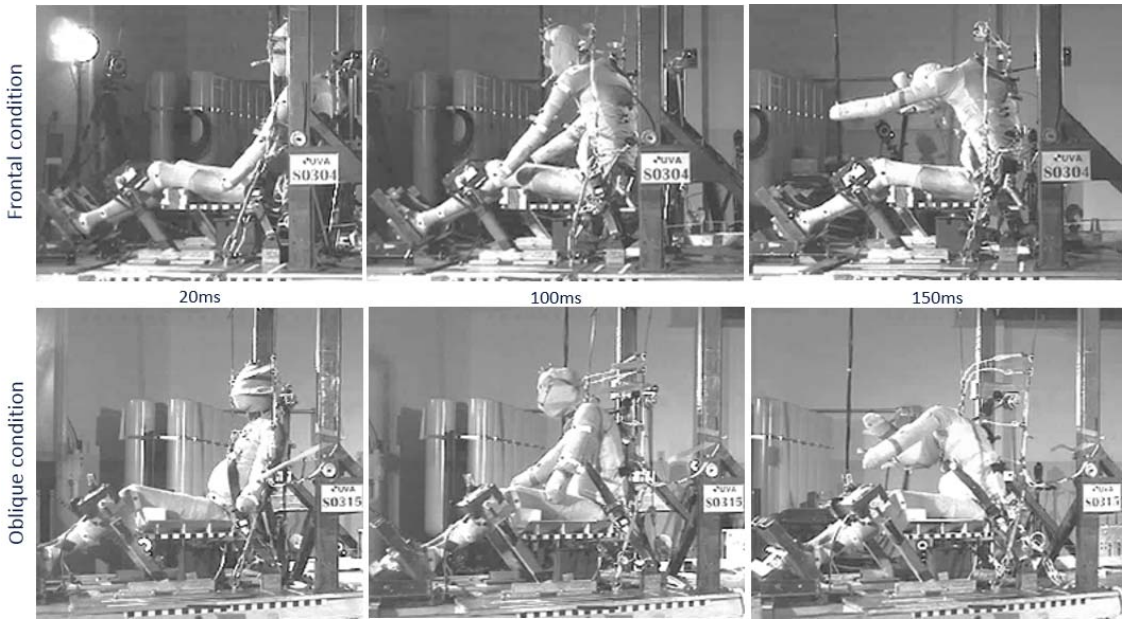

Fig. 6. Representative driver side still frames from high-speed imager for test S0304 frontal (*upper*) and S0315 oblique (*lower*).

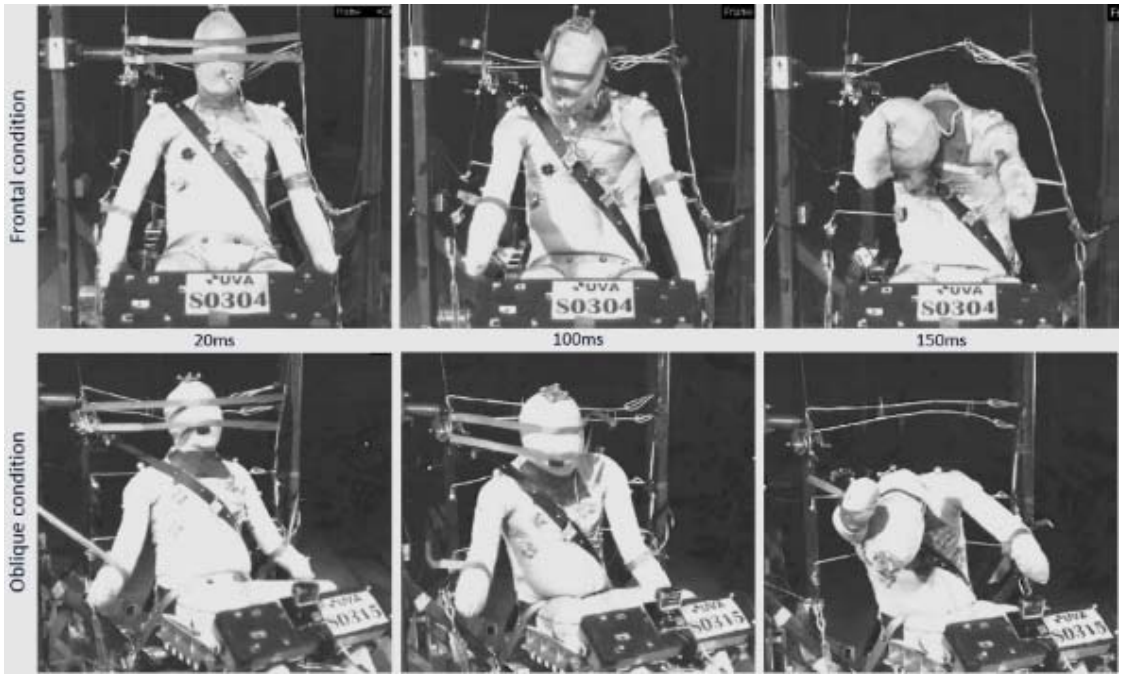

Fig. 7. Representative still frontal frames from high-speed imager for test S0304 frontal (*upper*) and S0315 oblique (*lower*).

Skeletal Kinematics

Figure 8 provides the mean peak displacements of each measured location for the eight PMHS in both the positive and negative X-axis, Y-axis and Z-axis directions (refer to the buck coordinate axes in Fig. 4, where the positive X-axis is forward, the positive Y-axis is to the occupant's right and the positive Z-axis is downward). As expected, all spinal measurement sites moved more laterally in the oblique condition as compared to the full frontal condition. This difference in peak lateral motion for the two test conditions was found to be statistically significant (Wilcoxon rank-sum test $p<0.05$).

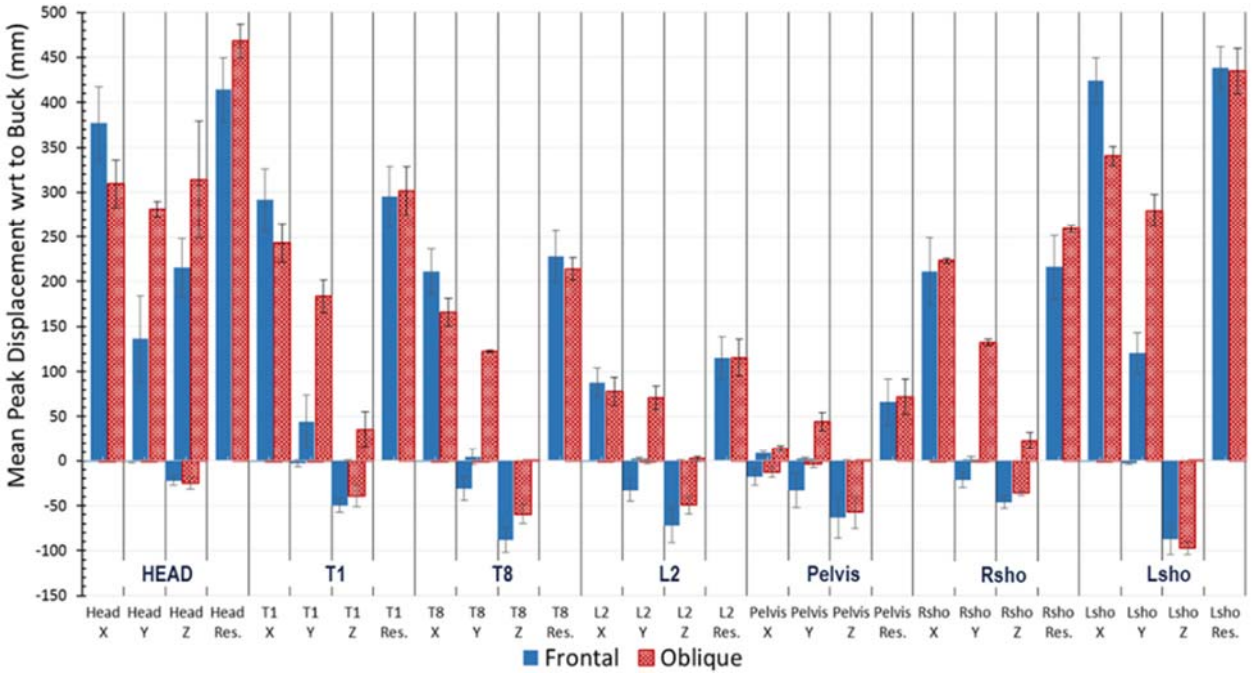

Fig. 8. Mean peak X-axis, Y-axis, Z-axis and resultant displacements with respect to the buck coordinate system +/- 1 S.D.

The resultant displacements of the head and Y-axis measurements of the shoulders were also in the oblique condition. Figure 8 provides the mean peak resultant displacements for each measured location in both the positive and the negative X-axis, Y-axis and Z-axis directions.

The average trajectory for the five subjects in GS2 and three subjects in GS3 at each measured skeletal location is illustrated in Fig. 9. More specifically, Fig. 9 provides lateral, posterior and superior 2D projections of the 3D spine shape and positions occurring during the test. An overhead view of the trajectory of each shoulder is also provided in Fig. 9. All 2D views are provided by projecting the 3D anatomical kinematic data onto the desired 2D reference frame of interest with respect to the buck for each condition (e.g. X-Z plane, Y-Z plane and Y-X plane). Note that there were differences in the average GS2 and GS3 subject initial position. This was due to variations in subject anthropometry and seated posture. In order to compare GS2 and GS3 average motion, the initial location of the pelvis was aligned in Fig. 9.

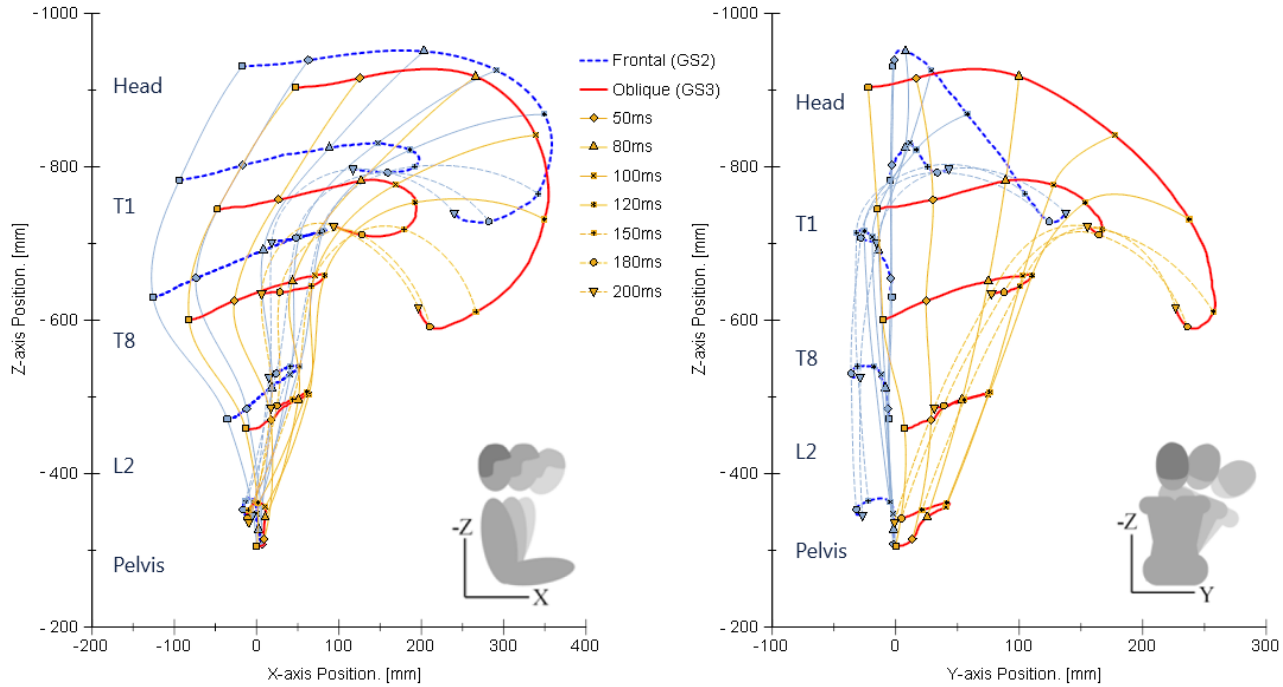

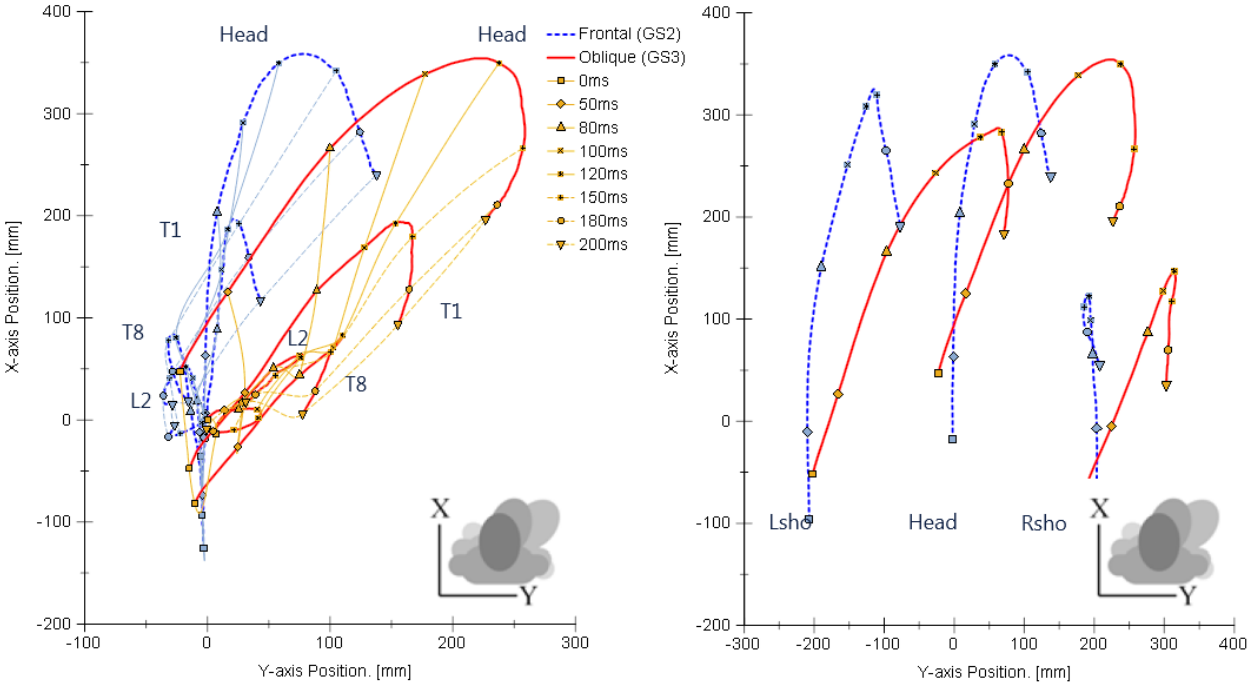

Fig. 9. 3D spine shape and position. Provided views are lateral (*upper left*), posterior (*upper right*), overhead views without shoulders (*lower left*) and head with shoulders (*lower right*).

Skeletal Displacement Corridors

Figures 10–13 illustrate the generated displacement corridors for the selected measurement locations in both frontal and oblique conditions. For each measurement location, corridor plots are provided for the X-axis, Y-axis and Z-axis displacements relative to the buck. Specifically, each corridor plot provides the calculated average curve and the ±1 S.D. corridor constructed around the average. More displacement is observed in the Y-axis direction (Fig. 10-13) of the oblique condition due to the lateral component of the buck acceleration.

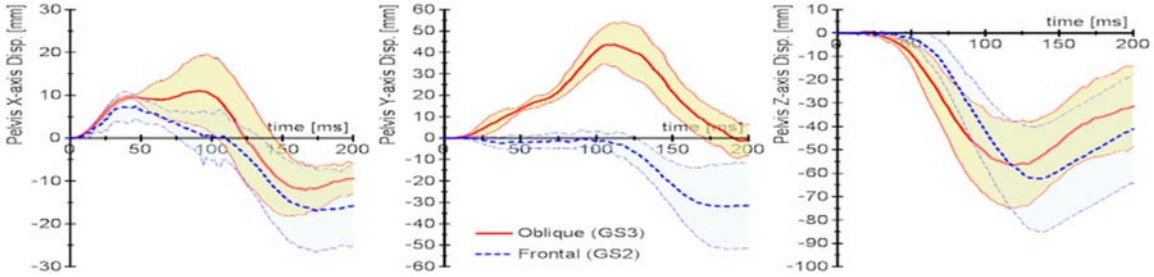

Fig. 10. Displacement corridors for the Pelvis.

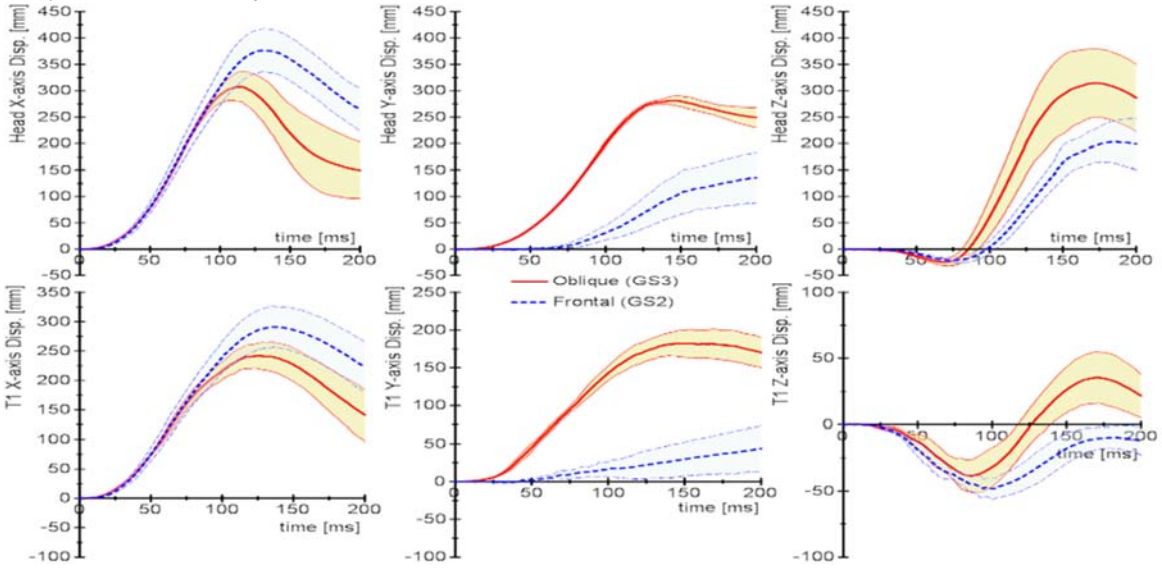

Fig. 11. Displacement corridors for the head and T1.

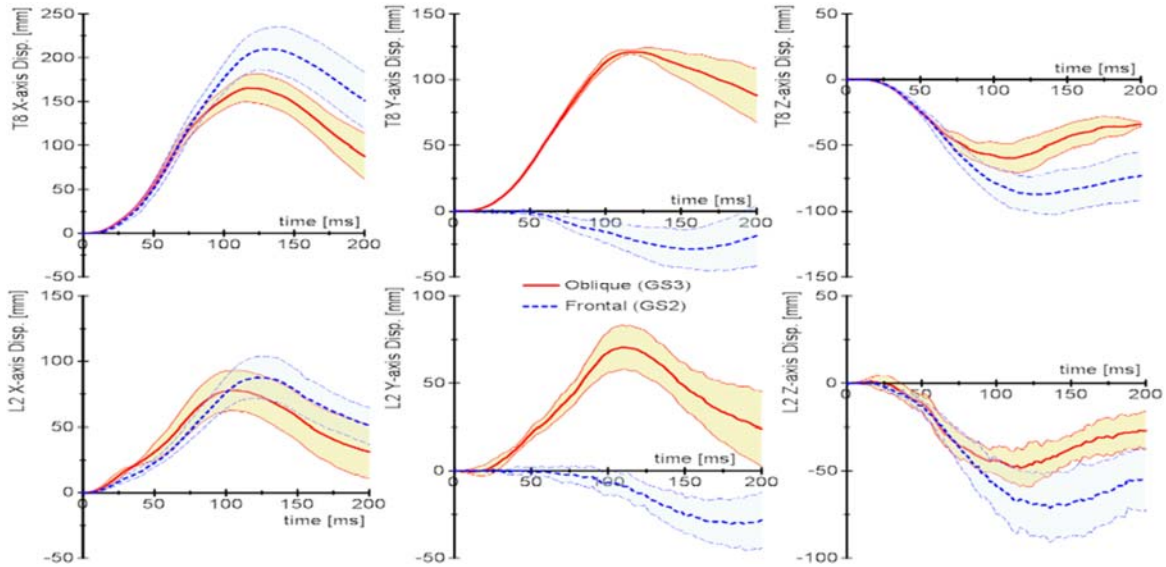

Fig. 12. Displacement corridors for the T8 and L2.

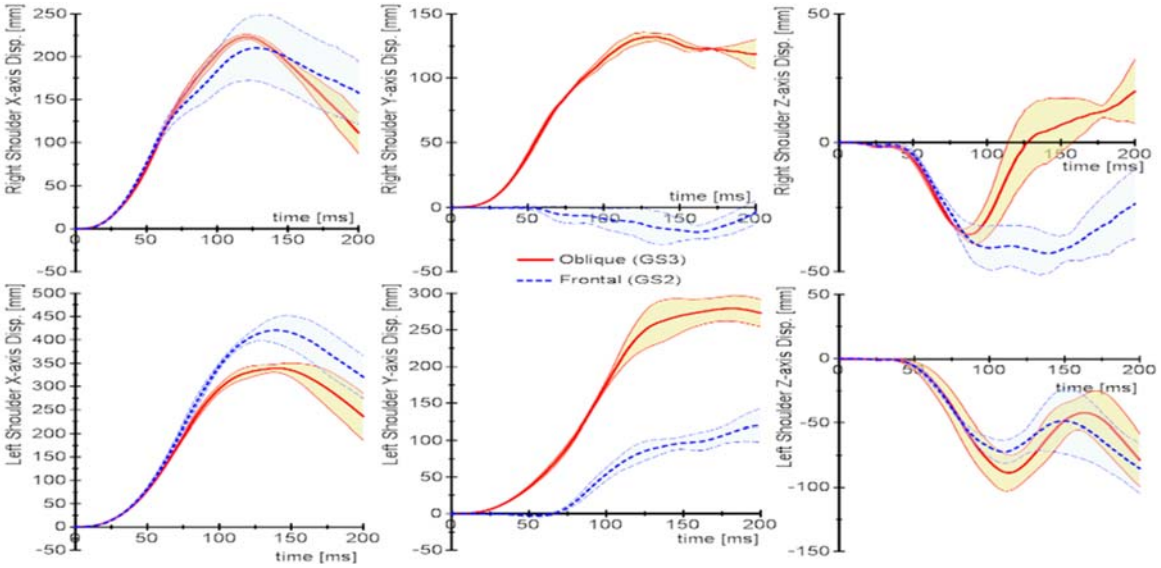

Fig. 13. Displacement corridors for the left and right shoulders.

Anterior Rib cage Deformation

For the oblique condition, thoracic deformation was greater at inferior (lower left and right) measurement locations compared to superior (upper left and right) locations. The oblique condition exhibited greater overall peak deflections compared to the frontal condition. However, this finding was not found to be statistically significant (Wilcoxon rank-sum $p>0.05$). Figure 14 presents the mean peak deflection of the anterior rib cage (sternum, upper left, upper right, lower left, and lower right) and the mean peak resultant relative to the T8 (i.e. spine) coordinate system in the X-axis, Y-axis and Z-axis directions.

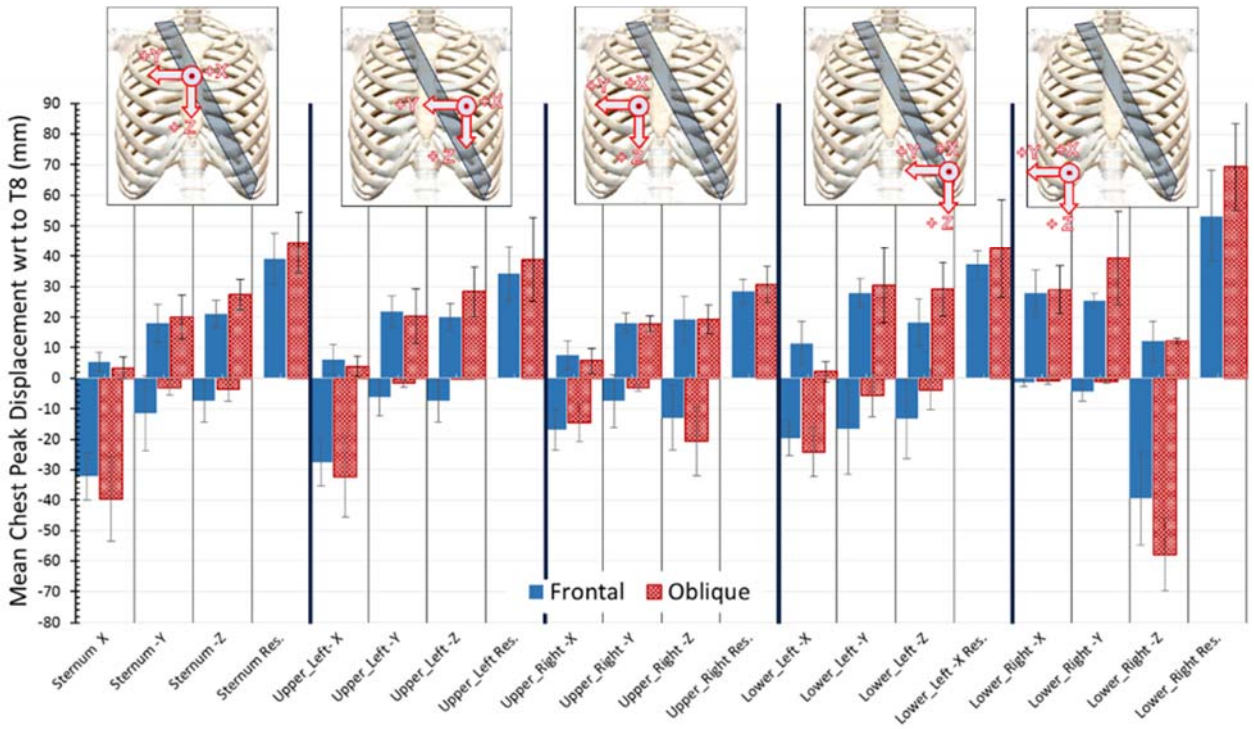

Fig. 14. Mean peak X-axis, Y-axis, Z-axis and resultant thorax deformation relative to the T8 (i.e. spine) coordinate system +/- 1 S.D.

Anterior Rib cage Displacement Corridors

Figures 15–17 illustrate the generated displacement corridors for the selected measurement locations in both frontal and oblique conditions. For each measurement location, corridor plots are provided for the X-axis, Y-axis and Z-axis in anterior rib cage displacements relative to the T8 (i.e. spine). Specifically, each corridor plot provides the calculated average curve and the one S.D. corridor constructed around the average.

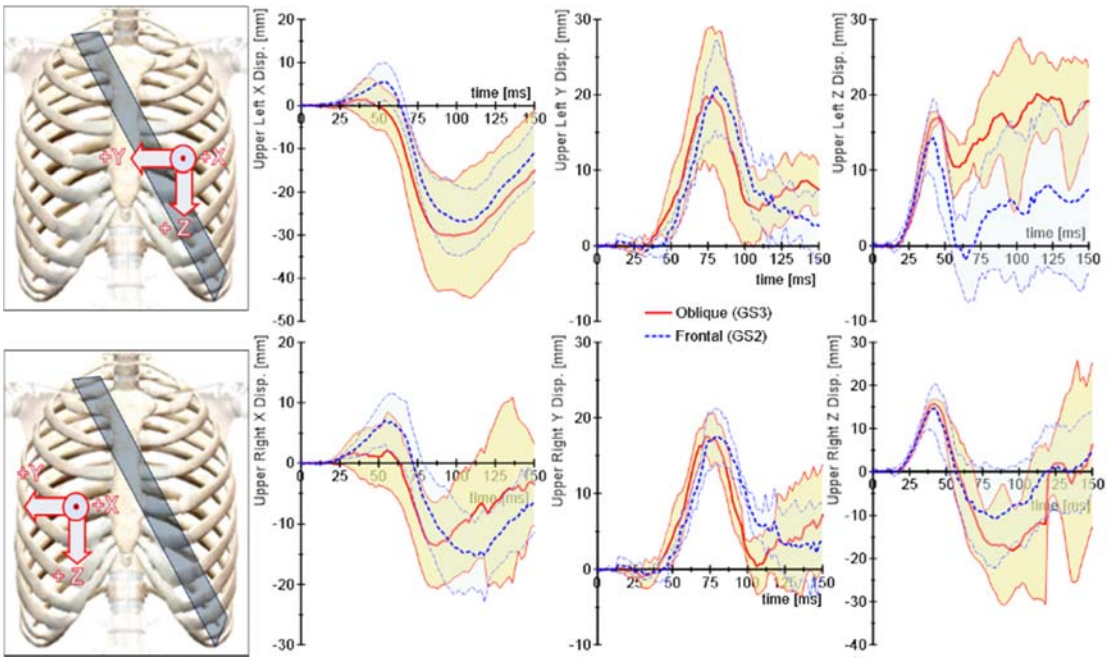

Fig. 15. Upper Left chest (UL) and Upper right chest (UR) displacement corridors relative to the T8 (i.e. spine) coordinate system X-axis, Y-axis, Z-axis, +/- 1 S.D.

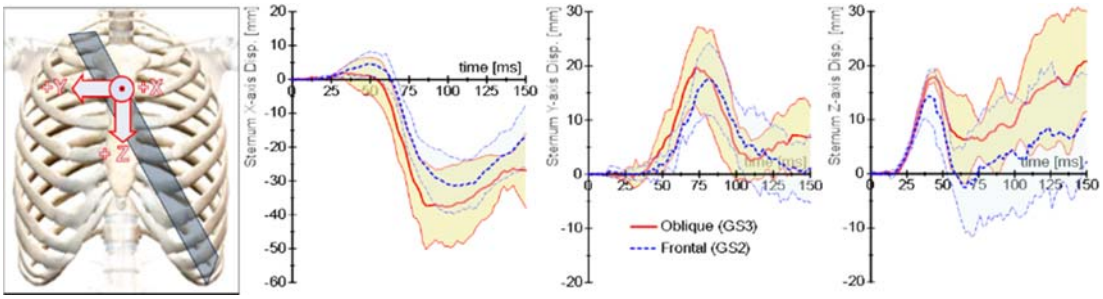

Fig. 16. Sternum displacement corridors relative to the T8 (i.e. spine) coordinate system X-axis, Y-axis, Z-axis, +/- 1 S.D.

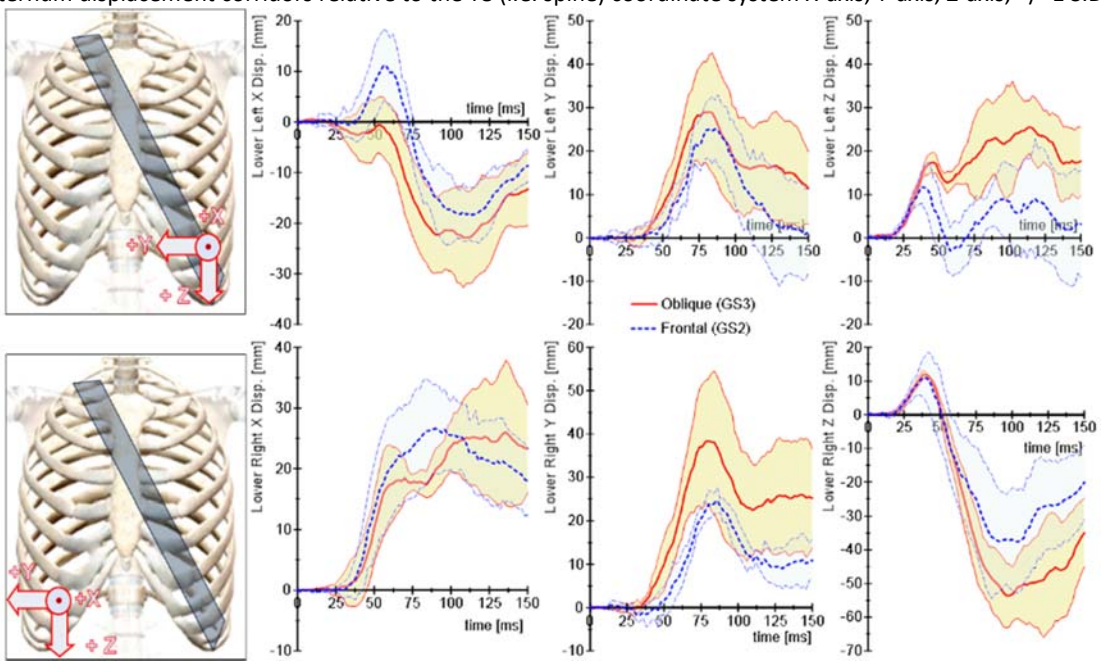

Fig. 17. Lower Left chest (LL) and Lower right chest (LR) displacement corridors relative to the T8 (i.e. spine) coordinate system X-axis, Y-axis, Z-axis, +/- 1 S.D.

Occupant Interface Measurements

Upper shoulder-belt loads were similar between the full-frontal and oblique conditions. The lower shoulder-belt force was 47% greater in the oblique tests caused by the oblique impact orientation and motion of the subject relative to the buck. The oblique condition also led to substantial asymmetry in the interface loads, with the right knee load 54% greater than the left. The full frontal condition peak left and right knee loads were similar.

Figures 18–20 illustrate the external force corridors in both frontal and oblique conditions and include the calculated average curve and the one S.D. corridor. Note that the reported measurements from the occupant interface load cells are the force or moment experienced by the occupant in the proper JSAE-211 polarity [4].

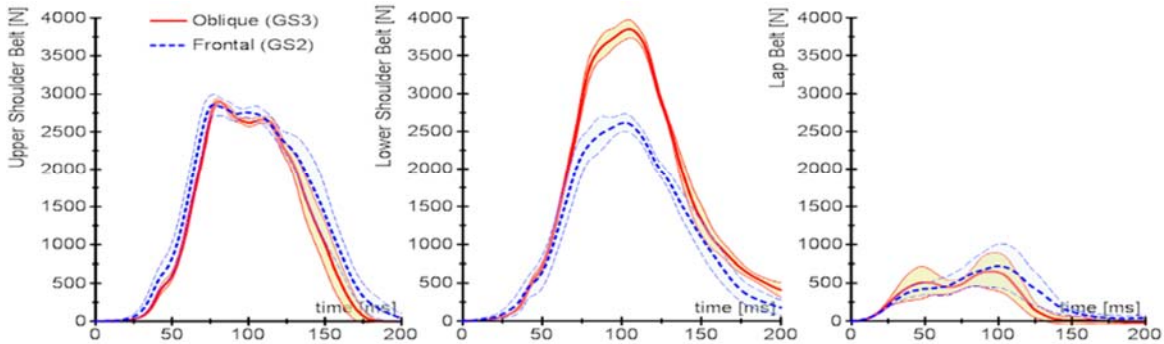

Fig. 18. Seatbelt forces time-history plots, +/- 1SD.

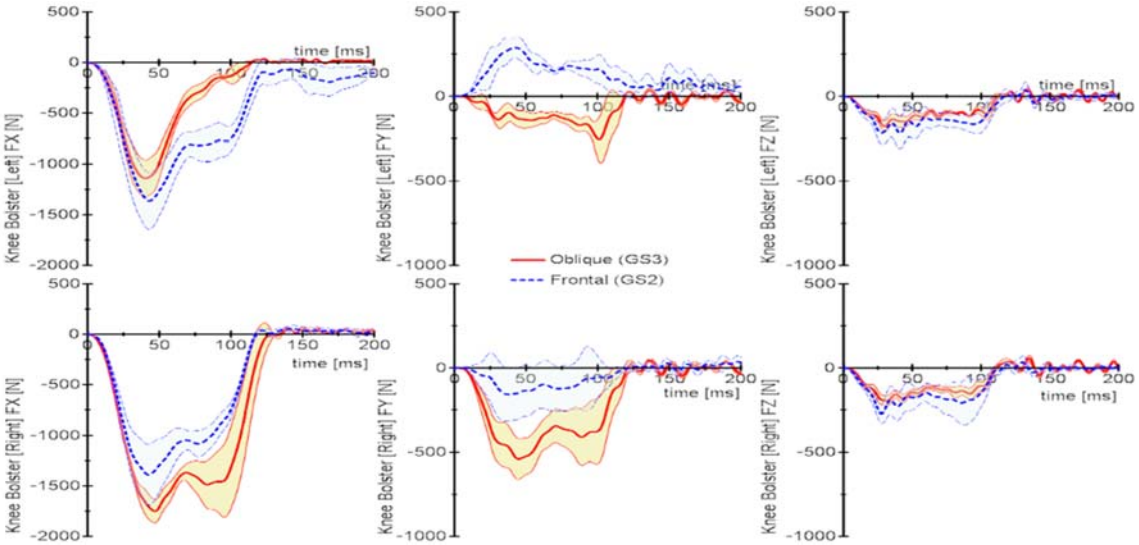

Fig. 19. Knee bolster left and right forces, time-history plots on the X-axis ,Y-axis and Z-axis, +/- 1SD

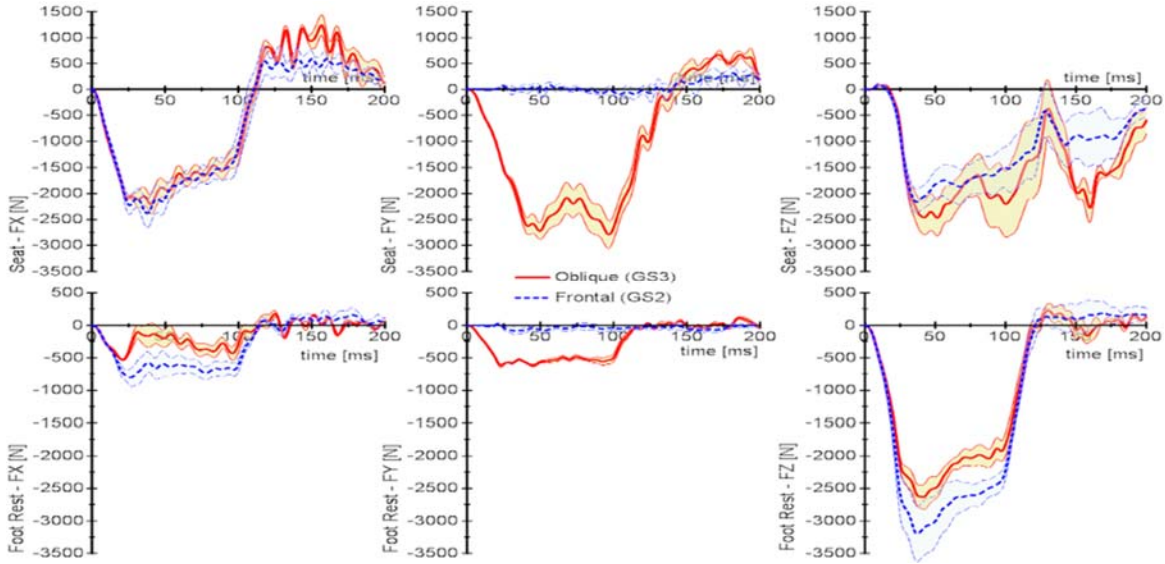

Fig. 20. Seat forces and footrest forces, time-history plots on the X-axis, Y-axis and Z-axis, +/- 1SD.

IV. DISCUSSION

The 3D displacement response of the spine and chest deflection of eight tested PMHS was recorded in tests with well-controlled conditions and comprehensive measurement of subject motion. The collected responses were well-behaved and revealed repeatable and consistent displacement characteristics occurring across all tested subjects in each respective test condition. In both the frontal and oblique conditions, displacement magnitude was greatest in the positive X-axis direction and was observed to be the highest at the head, with progressively decreasing magnitudes occurring at inferior locations along the spine, from T1 to the pelvis, as would be expected given the aggressive restraint of the pelvis and lower extremities. All locations along the spine moved upward (negative Z-axis direction) during the test with the exception of the head and shoulders, which moved downward (positive Z-axis direction) after an initial upward movement. In the frontal condition, the predominant spinal displacements were observed to occur, as expected, within the sagittal (X-Z) plane, but substantial displacements also occurred perpendicular to the sagittal plane (coronal Y-Z plane). The oblique condition generated substantially more lateral movement (Y-axis displacement) than was observed in the frontal impact condition as seen in Fig. 9. It was also observed that the resultant head displacement was greater in the oblique condition, in spite of the fact that the frontal subjects' statures were slightly greater than those of the oblique condition subjects, at 1.78 m and 1.74 m, respectively. This would indicate that factors associated with the oblique condition allow for greater head displacement when compared to that of a standard frontal impact for the same acceleration. Previously reported near-side oblique tests conducted with similar impact

angle and acceleration produced similar maximum average resultant head displacement with approximately 500 mm reported in the previous study [9] and 468 mm in the current study (Fig. 8).

Thoracic deformation in the oblique condition was more pronounced at the inferior measurement locations when compared to the superior locations, which may be related to the higher lower shoulder-belt loads compared to the frontal condition. The mean resultant thoracic deflection was also greater in the oblique condition than in the frontal condition at each of the thoracic measurement locations, though this difference was not statistically significant. Differences in thoracic deformation between the oblique and frontal conditions appear to correlate with the lower shoulder-belt loads and torso kinematics, though the causal mechanisms at play are not yet clearly understood.

The Gold Standard 2 and 3 conditions were designed to non-injurious or minimally injurious conditions and intended to focus on the kinematics of the thorax in idealised vehicle environments. The subjects in these tests suffered either no or a relatively small number of rib fractures for PMHS tests, with a total of 11 fractures among the five PMHS in the GS2 condition and 14 fractures among the three PMHS in the GS3. The difference in the average number of fractures between the conditions was not statistically significant (GS2: 2.2 ± 3.2 fractures; GS3: 4.7 ± 4.0 fractures). The fractures experienced in the testing are not thought to substantially affect the kinematics and in the event that fractures did affect the kinematics of the PMHS, the fractures were similar in both conditions and would therefore be expected to have a similar effect.

A previous study attributed increased risk of rib fracture in near-side oblique frontal conditions to contact with interior side structures [10]. The current study, conducted without a surrogate door structure, did not investigate this injury mechanism. However, the increased lower shoulder-belt load and (not statistically significant) greater thoracic deflection and number of rib fractures for the oblique condition suggest that the direction of impact alone may increase rib fracture risk.

V. CONCLUSIONS

The current study utilised a well-controlled 30 km/h frontal impact condition and 30 km/h oblique impact condition in conjunction with an anatomical kinematic measurement methodology to provide 3D displacements of the head, T1, T8, L2, pelvis and shoulders. This study also provided chest deformation at the sternum, upper left, upper right, lower left and lower right rib cage measurement locations. Kinematic and chest deflection biofidelity corridors were also constructed for the five PMHS in the frontal condition and the three PMHS in the oblique condition. The collected responses were observed to be well behaved and revealed repeatable and consistent displacement characteristics occurring across all tested subjects. The results will be immediately useful for kinematic biofidelity assessments of both ATDs and computational models.

VI. ACKNOWLEDGEMENT

US Department of Transportation National Highway Traffic Safety Administration provided both technical and financial support via Cooperative Agreement No. DTNH22-09-H-00247. Note that the views expressed in this paper are those of the authors and not of the sponsors.

VII. REFERENCES

[1] Ash, J.H, Lessley, D. et al. Whole-Body Kinematics: Response Corridors for Restrained PMHS in Frontal Impacts. Proceedings of IRCOBI Conference, 2012, Dublin, Ireland.

[2] Lessley, D. Shaw, C.G. et al (2011) Assessment and Validation of a Methodology for Measuring Anatomical Kinematics of Restrained Occupants During Motor Vehicle Collisions. Journal of Biosensors and Bioelectronics, S1:002.

[3] Shaw, C. G., Parent, D. P. et al. Frontal Impact PMHS Sled Tests for FE TORSO Model Development. Proceedings of IRCOBI Conference, 2009, York, UK.

[4] Society of Automotive Engineers. (2003) Surface Vehicle Recommended Practice J211-1 –Instrumentation for Impact Test – Part 1 –Electronic Instrumentation. SAE, Warrendale, PA.

[5] Wu, G., van der Helm, F. C. T. et al. (2005) ISB recommendation on definitions of joint coordinate systems of various joints for the reporting of human joint motion--part II: shoulder, elbow, wrist and hand. Journal of Biomechanics, **5**(38): pp.981–92.

[6] Schneider, L. W., Robbins, D. H., Pflug, M. A., Snyder, R. G. (1983) Anthropometry of Motor Vehicle Occupants, Vol. 3, Specifications and Drawings. Report HS-806 717, UMTRI-83-53-2. UMTRI, Michigan, USA.

[7] Lessley, D. J., Crandall, J. R., Shaw, C. G., Kent, R. W, Funk, J. R. (2004) A Normalization Technique for Developing Corridors from Individual Subject Responses. Society of Automotive Engineers, Paper 2004-01-0288.
[8] Shaw, J. M., Herriott, R. G., McFadden, J. D., Donnelly, B. R., Bolte, J. H. (2006) Oblique and Lateral Impact Response of the PMHS Thorax. Stapp Car Crash Journal, 50: pp.147–67.
[9] Tornvall, F. V., Svensson, M. Y., Davidsson, J., Flogard, A., Kallieris, D., Haland, Y. (2005) Frontal impact dummy kinematics in oblique frontal collisions: evaluation against post mortem human subject test data. Traffic Injury Prevention, 6: pp.340-50.
[10] Iraeus J, Lindkvist M, Wistrand S, Sibgård E, Pipkorn B. Evaluation of Chest Injury Mechanisms in Nearside Oblique Frontal Impacts. Annual Proceedings of the Association for the Advancement of Automotive Medicine 2013;57: pp.183-96.

VIII. APPENDIX

Appendix A: PMHS Positioning.

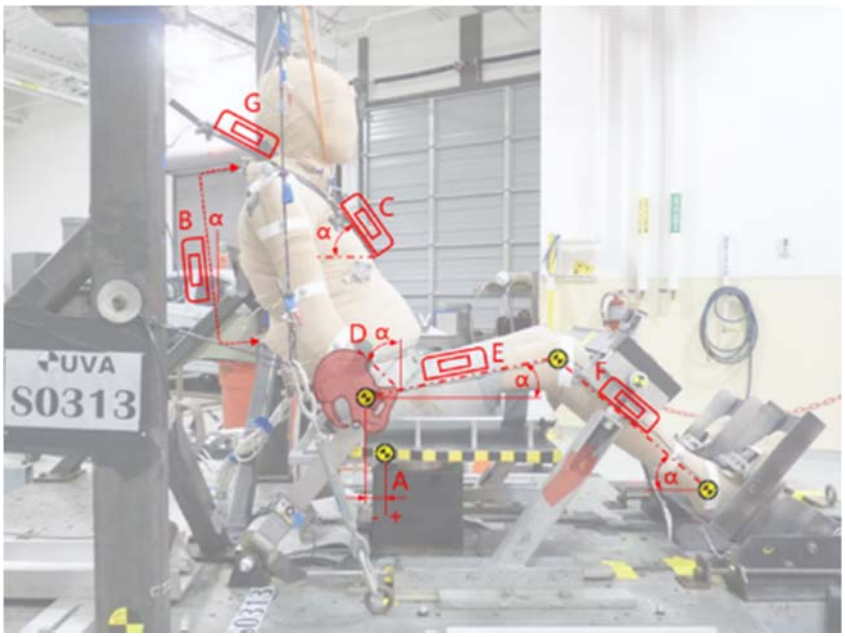

	TSTREF in NHTSA BioDB	A H-pt.	B Torso Angle	C Sternal Angle	D Pelvic Angle	E Femur Angle Right	F Tibia Angle Right	G Belt Angle
		mm	deg.	deg.	deg.	deg.	deg.	deg.
GS2	UVAS028	-14.0	-10.0	-18.0	nm	9.0	32.0	25.0
	UVAS029	-8.0	-10.0	-26.0	nm	11.0	32.0	26.0
	UVAS0302	-10.0	-6.0	-29.0	nm	12.0	36.0	26.0
	UVAS0303	10.0	-5.0	-17.0	nm	13.0	35.0	28.0
	UVAS0304	-15.0	-7.0	-30.0	nm	12.0	34.0	26.0
GS3	UVAS0313	-13.0	9.0	31.0	nm	13.0	42.0	32.0
	UVAS0314	-14.0	7.0	20.0	nm	5.0	42.0	29.0
	UVAS0315	-15.0	9.0	14.0	nm	11.0	39.0	31.0
GS2 average		-7.4	-7.6	-24.0	nm	11.4	33.8	26.2
GS3 average		-14.0	8.3	21.7	nm	9.7	41.0	30.7

nm – not measured

Notes

A] Horizontal displacement of the right H-point relative to the standard position for the Hybrid III dummy H point with the Taurus passenger seat in the mid-position. Negative values indicate further away from the footrest.

B] Angle of a line through the T3 and L1 spinous processes.

C] Angle of a plate screwed to the sternum.

E] Femur angle: angle of a line between the greater trochanter and the knee centre. *Lower angle in test S0314 due to shorter lower extremities.

F] Tibia angle: angle of a line between the knee centre and the ankle centre.

G] Angle of shoulder belt along the belt from the upper anchor to the shoulder.

Appendix B: PMHS Belt Position on Anterior Torso.

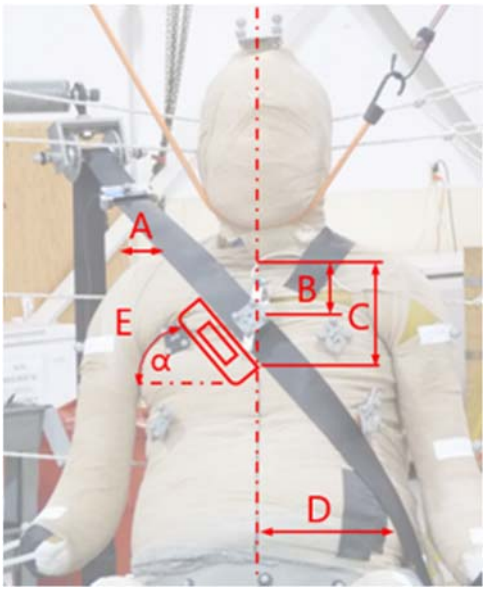

TSTREF in NHTSA BioDB		A Outer belt edge to acromion lateral border	B Sternal notch to upper belt edge	C Sternal notch to lower belt edge	D Inner belt edge from the midline at the level of the intersection of the 7th rib and the lower ribcage border	E Angle of upper belt edge at midline
		mm	mm	mm	mm	deg.
GS2	UVAS028	10	65	138	142	46.2
	UVAS029	20	68	145	nm	48.5
	UVAS0302	20	72	nm	nm	49.0
	UVAS0303	55	58	nm	nm	48.0
	UVAS0304	45	82	nm	nm	47.0
GS3	UVAS0313	51	48	nm	nm	46.0
	UVAS0314	51	48	nm	nm	45.0
	UVAS0315	45	70	nm	nm	47.0

nm – not measured